EROSION OF FROZEN GASES BY MeV ION BOMBARDMENT

By

HAROLD K. HAUGEN, B. Sc. (PHYSICS)

PART A: MCMCASTER (OFF-CAMPUS) PROJECT*

A Report

Submitted to the School of Graduate Studies

in Partial Fulfilment of the Requirements

for the degree

Master of Engineering

Department of Engineering Physics

McMaster University

Hamilton, Ontario, Canada

September 1978

* One of two project Reports: The other part is designated PART B: ON-CAMPUS PROJECT

MASTER OF ENGINEERING (1978) MCMASTER UNIVERSITY
Department of Engineering Physics Hamilton, Ontario

TITLE: Erosion of Frozen Gases by MeV Ion Bombardment

AUTHOR: Harold K. Haugen, B. Sc. (Acadia)

SUPERVISOR: Dr. J.A. Davies, Solid State Science Branch, Chalk River Nuclear Laboratories, Chalk River, Ontario, Canada KOJ 1JO

NUMBER OF PAGES: viii, 62

ABSTRACT

Recent measurements of the sputtering of frozen gases by MeV ions gave yields several orders of magnitude greater than predicted by collision cascade theory. Only a "thermal spike" model, invoking a coupling of electronic excitation to nuclear motion, agrees qualitatively with experimental results. Yields of 300 keV to 2 MeV ions ranging in mass from 4 a.m.u. to 40 a.m.u. were investigated for ice, Kr and Xe films in the temperature range of 15°K to 120°K.

ACKNOWLEDGEMENTS

I wish to thank my supervisor, Dr. J.A. Davies, for his direction of this research. I also wish to extend a special thanks to Dr. J. Bottiger[a] for his close collaboration and help. Thanks are also extended to Dr. N. Matsunami[b] for computer simulation related to this study, and to Dr. J. L'Ecuyer[c] and Dr. R. Ollerhead[d] who were involved in an earlier stage of the project.

J. Lindhard[e], Dr. D. Cherns[f] and Dr. P. Townsend[g] are acknowledged for interesting discussions during the course of the work.

(a) Institute of Physics, University of Aarhus, Denmark
(b) National Research Council Postdoctoral Fellow on leave from the Crystalline Materials Science Department, Nagoya University, Japan
(c) Short-term visitor from the Nuclear Physics Department, Université de Montréal, Quebec
(d) Department of Physics, University of Guelph, Ontario
(e) Institute of Physics, University of Aarhus, Denmark
(f) Department of Metallurgy, Oxford University, England
(g) School of Mathematics and Physical Sciences, University of Sussex, England

TABLE OF CONTENTS

I. INTRODUCTION

The sputtering, or ejection process by ion impact on a metallic or covalently bonded solid, is typically described by an atomic collision model. Sputtering yields are normally well accounted for by Sigmund's theory[1], based on nuclear collision cascades set up in the solid. In contrast, recent measurements of the sputtering of frozen gases by MeV ions gave yields several orders of magnitude larger than predicted by collision cascade theory.

An experimental study was hence initiated to investigate possible mechanisms. Among the potential mechanisms considered were target-heating effects, Coulomb explosion, and "thermal spikes" (localized regions of the solid where an ion deposits sufficient energy to transform the surrounding lattice to a "high temperature" state). Investigations by Davies et al.[2] showed that neither of the first two mechanisms was valid, but that the third was supported by experimental results. It should be pointed out that this is a surprising result, since the amount of energy deposited in nuclear collisions by ions of MeV energies is extremely small. However, the energy transfer to electronic excitation of lattice atoms is large, and

hence an electronic-nuclear coupling mechanism must be invoked as part of the model.

This work represents a detailed preliminary investigation of the "thermal spike" as applied to a high energy ion-solid interaction. The physical conditions implicit in a high energy density regime elude precise description by equilibrium physics. In fact, past quantitative calculations are subject to considerable controversy. This present work serves to show that in the case of bombardment of frozen gases by MeV ions only a thermal phenomenon qualitatively explains the results; but beyond a simple model and simulation, quantitative calculations will not be attempted here.

Such a study not only serves to give insight into a fundamental problem in atomic collisions, but is also of considerable practical interest. The erosion of frozen gases by particle flux is important in astrophysical phenomena, and cryogenic surfaces in vacuum systems may have large amounts of condensed gas. A particular case of technological importance is the use of superconducting magnets to confine thermonuclear plasmas.

II. THEORY

The interaction between an energetic charged particle and a target atom is typically described by a cross section. Hence probability concepts lie at the foundations of measurement processes in atomic collisions. It is thus impossible to predict "a priori" the exact nature of the interaction of an individual ion with the target. However, since a large number of particles are involved in any single measurement, an average is obtained whose precision can be estimated with Poisson statistics.

2.1 Stopping Cross Sections

Figure 1(a) illustrates the energy loss of a charged particle in penetrating a solid of thickness ΔX. The interaction is in general complex, depending on projectile, target and energy regime, the quantity of interest is the stopping power of the target defined by:

$$\frac{dE(E)}{dX} = \lim_{\Delta X \to o} \frac{\Delta E}{\Delta X} \qquad (1)$$

From a microscopic point of view the expectation value of the energy loss may be described in terms of the probabilities, P_i, for various interactions. With N, the number density of target atoms, the stopping power becomes:

$$\frac{\langle \Delta E \rangle}{\Delta X} = \sum_i T_i P_i = N \int T \, d\sigma \qquad (2)$$

where T_i is a particular energy transfer to a target atom and, $d\sigma$, the continuum analog of P_i - the differential scattering probability.

The integral above is termed the stopping cross section, S(E), which is in general a more useful quantity than the stopping power, because of the normalization to a single atom. This is significant in the present work since the interatomic spacing in frozen gas films is not known exactly, and hence the thicknesses are quoted in terms of the number of atoms per square centimeter.

2.2 Energy Loss Processes

A charged particle interacts with a solid mainly by the following processes:

(1) excitation of target atoms

(2) Coulomb collisions with target nuclei

(3) photon emission

(4) nuclear reactions

The last two need not be considered here - they are important at very high energies. Also the ratio of the electronic to nuclear stopping cross sections is generally large for MeV ions.

Although the electronic and nuclear components are correlated, it is usually a satisfactory approximation to separate their contributions.

2.2.1 Inelastic Energy Loss - Electronic Excitation

Figure 1(b) indicates the total stopping cross section for a proton in silicon on a logarithmic scale. Although this pertains to a particular ion-solid combination, the shape of the curve is general. Only at very low velocities does the nuclear stopping make any significant contribution to the total.

Generally speaking, classical or semi-classical calculations are feasible in the velocity region where the projectile moves more slowly than the electrons. This region has been treated in detail by Lindhard[3] and Firsov[4]. The quantum theory of stopping applies to high velocity ions and has been well summarized by Bethe[5], Fano[6] and Inokuti[7].

Presentation of electronic stopping in this work is based on experimental results as tabulated by Ziegler[8] or by Northcliffe and Schilling[9].

2.2.2 Nuclear Energy Loss

Whereas a universal electronic stopping power does not exist, Lindhard[10] has developed a universal nuclear

stopping curve in terms of a set of reduced paramenters.

When the scattering problem is solved by perturbation theory, valid for small Θ, and the result is extrapolated to large Θ; the differential scattering cross section, $d\sigma_n$, is obtained:

$$d\sigma_n = \pi a^2 \, (dt/2t^{3/2}) \, f(t^{1/2}) \qquad (3)$$

Here t is a reduced energy transfer, and $f(t^{1/2})$ is the universal screening function indicated in Figure 2(a).

The screening function, the reduced energy parameter ε, and the reduced range parameter ρ may be used to define a universal nuclear stopping cross section, given by:

$$\left(\frac{dE}{d\rho}\right)_n = - Sn(\varepsilon) = \frac{1}{\varepsilon} \int_0^{\varepsilon} f(t^{1/2}) \, d(t^{1/2}) \qquad (4)$$

and illustrated in Figure 2(b). The dashed curves represent Lindhard's low velocity approximation to electronic stopping for two ion-solid combinations.

In order that a comparison may be made with the general features of total stopping in Figure 1(b), $\varepsilon = 1$ corresponds to an energy of about 10^{-3} MeV for a proton in silicon. For $\varepsilon \gtrsim 10$ the nuclear stopping drops off approximately inversely with energy.

It should be pointed out that although the nuclear stopping may be much less than the electronic contribution,

it cannot necessarily be ignored. The nuclear component represents a direct lattice excitation, whereas the electronic contribution has an associated coupling, and hence a much reduced efficiency for "thermal spike production".

2.3 Sigmund Sputtering Theory

Sigmund assumes sputtering to result from cascades of atomic collisions initiated by a penetrating ion. The ejection process is indicated schematically in Figure 3(a)(1).

An integrodifferential equation is developed for the yield from a general Boltzmann transport equation. Figure 3(b) represents the damage and range distributions for a particular ion-solid combination with a ratio of the projectile to target mass of 8:1. The shaded region represents the sputtering of target atoms. In constant, yields greatly exceeding those predicted by cascade theory result from evaporation from a "thermal spike" region, as illustrated in Figure 3(a)(2).

2.4 The "Thermal Spike" Model

2.4.1 General Comments

It has often been suggested that when the energy density in a collision cascade is sufficiently high, the

cascade volume may best be described as a high temperature region or "spike", which cools mainly by conduction to the surrounding lattice. Such a model is supported by numerous experimental data, and since the general features have recently been treated in detail by Kelly[11], they will not be repeated here.

2.4.2 A Cylindrical Energy Spike

Whereas most thermal spike phenomena refer to cases where the nuclear energy deposition is large, and where the ion is stopped in the near-surface region; it is proposed, for calculation of erosion yields, that MeV ions deposit energy in a semi-infinite cylindrical volume as illustrated in Figure 4. The radius of the hot cylindrical region of temperature T_m, is r_o. The thermal diffusivities of xenon and beryllium are indicated by K_1 and K_2 respectively, and T_o is the substrate temperature. A thin (< 50 Å) layer of copper serves as an energy marker in the Rutherford back-scattering spectrum.

The following familiar heat equation applies to the cylindrical geometry:

$$\frac{\delta T}{\delta \tau}(r,z,\tau) = \frac{K}{r}\frac{\delta}{\delta r}\left\{r\,\frac{\delta T}{\delta r}(r,z,\tau)\right\} + K\,\frac{\delta^2 T}{\delta Z^2}(r,z,\tau) \qquad (5)$$

where T is the temperature of the spike; r the distance from the ion track; τ the time after the initial energy deposition; Z the depth below the surface; and K the

thermal diffusivity.

The above is subject to the following boundary condition:

$$T(r,\ell,\tau) = T_o \quad \text{(the substrate temperature)} \tag{6}$$

and to the following initial conditions:

$$T(r,z,o) = T_m \quad \text{for } r \leq r_o \tag{7}$$
$$= T_o \quad \text{for } r > r_o$$

In the limit of small r_o, the following solution is found:

$$\frac{T(r,z,\tau) - T_o}{T_m - T_o} = T^*(r,z,\tau)$$
$$= \frac{\pi}{4}\frac{r_o^2}{K\tau} e^{-r^2/4K\tau} \operatorname{erf}\left(-\frac{Z}{2\sqrt{K\tau}}\right) \tag{8}$$

With $Z = \ell$ the surface temperature is obtained:

$$T_s(r,\tau) = T_o + (T_m - T_o)\, T^*(r,\ell,\tau) \tag{9}$$

If $\ell << 2\sqrt{K\tau}$, $\operatorname{erf}(\ell/2\sqrt{K\tau}) \simeq \frac{2}{\pi}\frac{\ell}{2\sqrt{K\tau}}$ and the temperature is proportional to the target thickness, ℓ.

The erosion rate is then determined by assuming a Boltzmann distribution in the spike volume. According to kinetic theory the number of atoms leaving the surface is given by:

$$\emptyset = \frac{1}{4} n \bar{v} \text{ atoms/cm}^2 \text{ - second} \tag{10}$$

where n is the density of atoms in the gas phase and $\bar{v}$ is the mean velocity. From familiar expressions for the pressure, p, and the average velocity one obtains:

$$\phi = 3.51 \times 10^{22} \frac{p}{\sqrt{mT}} \text{ atoms/cm}^2 \text{ - second} \qquad (11)$$

where p is in mm Hg, m in atomic mass units, and T is the absolute temperature.

2.5 Principles of Backscattering Spectrometry

Measurements of erosion yields are conveniently determined by Rutherford backscattering analysis. Elastic backscattering results from close nuclear Coulomb collisions, and the associated energy loss can be derived from principles of energy and momentum conservation. The electronic energy loss represents a continuous slowing down of the particle and is responsible for the depth-energy spectrometry.

The general features are outlined in Figure 5, with a typical thick target spectrum shown in the lower right hand corner. The energy of a particle scattered from a depth t is given by:

$$E(t) = K^2 \left(E_o - \int_o^t N\, S(E)\, dt\right) - \int_{t/\cos\phi}^{o} N\, S(E_1)\, dt \qquad (12)$$

where K^2 is the kinematic factor of the collision, N is the atomic number density, and S(E) the stopping cross section.

Backscattering yields of MeV light ions used for materials analysis are essentially described by the differential scattering cross section given by Rutherford. The number of atoms per square centimeter of an element in

the target may be determined from the Rutherford relation, and the product of the detector solid angle and detector efficiency.

It has recently been pointed out[12], however, that in regimes which had previously been considered totally Rutherford, there exists an important correction for electron screening. This correction has been applied to data analysis in this work.

III. EXPERIMENTAL TECHNIQUE

Backscattering spectrometry and thin film techniques were applied. The frozen gas films were deposited in situ on a cold backing of beryllium, having a thin (< 50 Å) copper layer. In previous studies[2] Al and Si substrates had also been used.

The target chamber is indicated in Figure 6, showing the 2-axis goniometer for sample manipulation, and the surface barrier detector at a 150° scattering angle. The goniometer head was connected to a closed cycle cryogenic cooler and ohmic heater, allowing the temperature to be varied from $\lesssim$ 20 K to 300 K. With the whole cryoshield maintained near 20 K, the pressure near the surface was $\lesssim 10^{-10}$ torr.

A Nuclear Data ND4420 and ADC were used for visual display of the backscattered spectrum. A Conuclear Multi-Scaler (C 7027) recorded real time, digital current (i.e. dose), and the number of counts in the peak from the frozen gas film.

Figure 7 shows a typical spectrum from a xenon layer, before and after prolonged bombardment. As was typical of xenon, Figure 7(b) indicates very nonuniform erosion. When sputtering with helium and nitrogen the

experiment was run in a cycling mode, with the beam continuously on target. The contents of the scalers were output after each incremental dose. The data analysis is illustrated in Figure 8, which essentially indicates the change in thickness as a function of bombardment dose. By a least squares fitting of the data points, the erosion yield may be determined. Since this mode involves an acquisition dead time for scaler output, a correction has been applied which is typically of the order of 5%. For heavier ion bombardment, the sputtering ion may not be used for analysis, either because the ion does not backscatter at 150° or because of detector degradation from radiation damage. In these cases sample thicknesses before and after bombardment were determined with a 1 MeV He beam.

Since the structure of the frozen gas films is unknown, parameters such as film thickness, deposition rate and film deposition temperature were kept constant. Although structure may depend on vacuum conditions of a particular day, the reproducibility of results indicated that this was not a major problem.

After mass separation, two 1 mm apertures provided beam collimation. Greater uniformity of ion flux on the film was ensured by rastering the beam over a 1 mm aperture in front of the target. With the deflection plates positioned after the first aperture, the area intercepted on

target was calculated from geometrical arguments, assuming the first aperture to represent a point source. Since the calculation is not exact, some absolute error is expected in the erosion yields. Nevertheless, reproducibility was excellent, and only relative changes are significant in elucidating the various physical mechanisms.

IV. RESULTS

Sputtering yields were found to be very dependent on the target film and the incident ion. It should be pointed out that measurements carried out at different beam current densities (up to 10^{-7} A/mm^2) gave the same results. All data presented in the tables has been corrected for cross section enhancement with energy loss and for acquisition dead time, where applicable. Table I summarizes the recent results for the sputtering of ice.

4.1 Sputtering of Ice

4.1.1 Helium Irradiation

a) Thickness Dependence of the Yield

The thickness dependence of the sputtering yield of 1 MeV ^{4}He on ice is shown in Figure 9. A small negative thickness coefficient is evident for films up to 500×10^{15} molecules/cm^2. Thereafter the yield rises sharply to a saturation level $\sim 750 \times 10^{15}$ molecules/cm^2, although some evidence exists for a slow decrease beyond this point.

b) Temperature Dependence

As illustrated in Figure 10 the sputtering yield also exhibits a small negative temperature coefficient up to about 60 K. Since the 20 K point represents three measurements taken on different days, the effect seems real. Beyond that point the yield rose with temperature up to 120 K, beyond which evaporation precluded further measurements.

c) Energy Dependence

The sputtering yield of ^{4}He on ice was found to be a monatonically decreasing function of energy. Figure 11 shows the sputtering yield to deviate from a direct scaling with the total stopping power. This became more evident in recent measurements tabulated in Table I (c), where the yield was rising at 300 keV, although the peak in the stopping power is near 600 keV.

d) Angular Dependence

Measurements of the angular dependence may yield some insight into the gross features of the ion-solid interaction. The sputtering yield was found to be an increasing function of the incidence angle (with respect to the surface normal), and is illustrated in Figure 12. The slope of the curve was found to be greater than a

$1/\cos\theta$ relationship and in fact scaled closely with a $1/\cos^2\theta$ dependence.

e) Dependence on Deposition Temperature

Since the base temperature ($\sim$ 20 K) may vary within a couple of degrees, it was desirable to investigate the effect of the temperature at which the film was deposited. A summary of results appears in Table I (e), giving some evidence for a small temperature effect but indicating that the effect is unimportant for small temperature changes.

4.1.2 Heavy Ion Results

The ^{14}N bombardment data, shown in Figure 11, indicates a direct scaling with electronic (or total) stopping power. More recent measurements, tabulated in Table I (f), verified the previous ^{14}N yields* and extended the investigations to ^{40}Ar where the nuclear stopping has risen from about 1% of the total stopping for 1 MeV ^{14}N to 15% of the total for 1 MeV ^{40}Ar; and at 300 keV ^{40}Ar deposits 30% of its energy in nuclear collisions. Whereas the nuclear stopping power is always

* Note that the more recent data was cross section corrected.

a decreasing function of energy, the ^{40}Ar results were also found to scale with electronic stopping (although not linearly): rising from S = 190 at 300 keV where (dE/DX) el 100 eV/10^{15} molecules/cm^2 to S = 910 at 1 MeV where (dE/dX) el has risen to about 160 eV/10^{15} molecules/cm^2.

4.2 Sputtering of Xenon

4.2.1 Helium Irradiation

a) Thickness Dependence of the Yield

Figure 13 shows a strong thickness dependence of 1 MeV ^4He sputtering of Xe. The yield rises sharply at small thickness and saturates around 200 X 10^{15} atoms/cm^2. This dependence is enhanced at 40 K since xenon sputtering exhibits a strong temperature dependence. The effect of an insulating SF_6 layer between xenon and the substrate is also indicated. Here the yield decreases with increasing xenon thickness but again tends to achieve a constant erosion rate at a thickness $\sim$ 200 X 10^{15} atoms/cm^2.

b) Temperature Dependence

The xenon sputtering yield was found to be a very strong function of the substrate temperature. Figure 14 shows the curve to rise sharply from $\sim$ 15 K with the yield increasing by an order of magnitude over a 30 K interval.

The strong temperature dependence coupled with the uncertainty in absolute temperature contribute to the possible error associated with the measurements. Above 45 K measurements could not be made since evaporation became a significant factor.

c) Energy Dependence

As seen in Figure 15, the erosion yield was found to scale with the total (or electronic) stopping power over the energy range of 400 keV to 2 MeV. Measurements were made with films thicker than 300 X 10^{15} atoms/cm^2 so that the thickness dependence was not a significant parameter.

d) Angular Dependence

As with the sputtering of ice, xenon films exhibited a strong angular dependence of the erosion yield for 1 MeV $^4He^+$ at 15 K. Figure 16 indicates that the dependence on the angle of incidence was again stronger than a $1/\cos\theta$ scaling. Measurements beyond 50° could not conveniently be made with the low temperature goniometer and cryoshield arrangement. As with all measurements of the sputtering yield of MeV ions on frozen gas films, angles of incidence greater than 5° were used to avoid possible texture effects (e.g. channeling).

4.2.2 Nitrogen and Argon Irradiation

Contrary to the direct scaling with total stopping power for ^{14}N on ice, yields for xenon scaled with nuclear stopping power as seen in Figure 15. At 400 keV the nculear stopping cross section is about 5% of the total and drops to about 1% at 1.5 MeV. In contrast, the nuclear stopping of He in Xe is less than 1% for all energies of bombardment. In order to investigate the correlation with nuclear stopping cross section, irradiations of xenon films with ^{40}Ar ions were performed.

The argon ion results, compared with nuclear and electronic stopping curves, for the ^{40}Ar - Xe combination are shown in Figure 17. The nuclear stopping cross section decreases from $\sim$ 35% of the total at 300 keV to $\sim$ 4% at 2 MeV. Nevertheless, the sputtering yield was found to be essentially independent of ^{40}Ar ion energy.

4.3 Helium Irradiation of Krypton

In order to ensure that atoms with similar electronic shell structure would exhibit similar erosion behaviour, krypton films were irradiated with 1 MeV ^{4}He at 20 K and 35 K. The sputtering yield rose from 9 atoms/ion to 25 atoms/ion at the higher temperature. The film thickness were similar for the measurements;

350×10^{15} atoms/cm^2 and 340×10^{15} atoms/cm^2 respectively.

V. DISCUSSION AND CONCLUSIONS

5.1 Limitations of Experimental Technique

This section serves to outline the various sources of uncertainty in the measurement of sputtering yields. A distinction must be made between absolute and relative errors, with the former estimated to be considerably greater than the latter in most studies.

As previously mentioned, the area being sputtered represents a major source of experimental error. Assuming the first of the collimating apertures a point source, represents a first approximation; geometrically a rough average. A consideration of beam optics and the collimation system demonstrates the dependence of the intercepted area of the target on the energy stability of the beam. Changes in steering for example, may affect the yield, but this should represent a small source of error in the cycling mode of data acquisition.

The accuracy of all absolute backscattering measurements relies on knowledge of the incident beam energy and the product of the detector solid angle and

detector efficiency. Also, a correction was made to the Rutherford cross section for electron screening, but uncertainties in backscattering analysis likely represent a small part of the total experimental uncertainty.

A more serious consideration is the condition of the thin films. The exact film structure is unknown and could conceivably be a sensitive function of the conditions of deposition, although experimental results gave no indication of this. Nevertheless, conditions for film deposition were maintained reasonably constant, although variations in the ambient vacuum conditions may represent a source of varying degree of contamination. Often a low initial sputtering rate was observed, indicating the effect of surface contamination.

Film uniformity will be discussed later in connection with the anomalous sputtering behaviour of ice. Texture effects were avoided by using a small tilt angle ($\sim 5°$) with respect to the perpendicular to the beam direction.

Since single channel analyzers and scalers were used for data acquisition, no dead time correction for the electronic components was applicable. However, in the

cycling mode of data acquisition the beam was on target during the time period for scaler output. The magnitude of the effect depends on the beam current density, but the correction applied was typically five percent.

5.2 Review of Possible Physical Mechanisms

Of all possible physical mechanisms, it was shown that only the thermal spike model is qualitatively in agreement with experimental results. Estimation of the macroscopic target heating effect was based on standard thermal conductivities of the substrate materials, and the steady state temperature rise was determined to be $\lesssim 10^{-3}$ K under normal conditions. This depends on the perfect condition of the substrate (e.g. no gaps between layers) so that verification that the sputtering yield was independent of current density provided an independent check.

The low positive to neutral sputtered particle ratio ($\leq 10^{-2}$), as well as the failure to explain the observed temperature dependence eliminated the Coulomb "explosion" model as the direct sputtering mechanism. The charged particle fraction had been determined by measuring the currents to the cryoshield under different bias conditions. However, this does not exclude the validity

of an indirect Coulomb mechanism, in that electronic excitation may set the lattice into motion. The details of the correlation of experimental results with the intuitive mathematical model of a cylindrical energy spike is presented below.

5.3 Evidence for a Thermal Spike Model

5.3.1 The Microscopic Model

The thermal spike model embodies the concept of a hot central core which cools by conduction (the radiation boundary condition may be shown to be insignificant) over times much longer than the time required to generate the gross features of the initial energy distribution. The flux of substrate particles contributing to the erosion depends on the surface temperature as given by equation (9). The flux as given by equation (11) is very strongly temperature dependent since the vapour pressure at the surface is an exponential function of the absolute temperature.

Numerical integration had been performed to estimate reasonable vlaues of the microscopic parameters. For ^{4}He incident on Xe a yield of 30 atoms per ion was obtained with a spike radius of 10 nm, with an intial temperature of 100 K and the substrate at 20 K.

The model also predicted that the significant fraction of the erosion occurred in the first few tenths of a nanosecond. Nevertheless, it should be pointed out that most thermal spike mechanisms discussed in the literature involve much shorter time scales, and conditions under which a significant fraction of the spike volume is ejected from the solid. In fact, the application of a thermal spike model to heavy ion bombardment of metals has recently been questioned[13], and correlated with a nonequilibrium effect associated with the nuclear stopping power at the surface. In contrast, MeV ion bombardment of frozen gases does not depend on the nuclear stopping (at least not directly), and takes place over sufficiently long time scales such that quasi-equilibrium conditions are expected to exist. Thus it is assumed that such studies may represent a convenient means of studying the spike mechanism.

5.3.2. Interpretation of the Temperature Dependence

The most convincing test of a thermal mechanism in the atomic ejection process is the temperature dependence of the yield. The temperature of the substrate establishes the heat sink for the dissipation of the cylindrical energy spike. Equation (8) gives the parameter $T^*(r,z,\tau)$ indicating the approach to equilibrium,

which for fixed spatial coordinates, is solely a function of time. As seen from equation (9) raising T_o increases the time period over which the temperature of the spike volume will be close to T_m. Hence the exponential dependence of the vapour pressure on the temperature of the solid leads to the prediction of a strong temperature dependence for the spike mechanism.

All ion-frozen gas combinations studied exhibited a strong temperature dependence of the erosion yield. Although ice films exhibited the smallest enhancement - approximately a factor of two - the description of their behaviour is expected to be more complicated, as discussed in a later section. Xenon, however, showed over a ten-fold increase for a 30 K increase in substrate temperature. Krypton too showed a strong temperature dependence with a three-fold increase over 15 K.

Thus investigations of the variation in yield with the substrate temperature strongly support a thermal spike model. Further evidence was obtained from investigation of the spatial heat transport, involving measurements of the thickness and angular dependence of the sputtering yield.

5.3.3 Characteristics of Spatial Energy Transfer

It has been shown that the temperature at the surface of the film scales linearly with the target thickness for sufficiently small thicknesses. For larger thicknesses it is intuitively expected that the surface temperature be relatively independent of film thickness, since for large l the heat dissipation of the near surface region will take place primarily radially through the frozen gas film.

Qualitative agreement was obtained with xenon sputtering, exhibiting a strong positive thickness coefficient for thin films, and a yield saturating at coverages of $\sim 200 \times 10^{15}$ atoms/cm^2. The erosion behaviour of ice films was essentially similar, although somewhat more complicated. The anomalies will be discussed later.

As pointed out earlier, an insulating SF_6 layer beneath the xenon film caused large enhancements in the erosion yield, especially at small thicknesses. This may in part be attributed to the reversed direction of heat transfer - from the SF_6 to the Xe. However, some limited evidence exists supporting the conclusion that the residual enhancement observed at greater coverages $\sim 300 \times 10^{15}$ atoms/cm^2 of xenon is due to an enhanced

diffusion mechanism, since Xe which diffuses into SF_6 will backscatter the ^4He with a degraded energy and not be counted in the xenon peak. It is expected that to a first approximation this effect is independent of xenon thickness. On the other hand, the large increase in yield at small Xe thicknesses must be attributed to the heat transfer from the SF_6 layer into the xenon film.

Measurements of the angular dependence of the yield provide another investigation of the spatial energy transfer. Based on the cylindrical energy spike it is expected that, as a first approximation, the yield would be directly proportional to the area of the initial spike volume on the surface; a $1/\cos\theta$ scaling, where θ is the angle of incidence with respect to the surface normal. However, both in the case of ^4He irradiation of ice and xenon films, the yields exhibited a dependence close to $1/\cos^2\theta$. Since the above approximation assumes a finite discontinuity in temperature at the initial radius of the cylindrical energy spike, r_o, for all time over which the erosion rate is significant; this is not a surprising result. If the enhancement in surface temperature for points outside the initial spike volume, as a result of the increased heat source in the near surface region, is sufficient, yields in excess of the $1/\cos\theta$ scaling may

reasonably be expected.

Hence macroscopie measurements of the heat transfer mechanism qualitatively support a thermal erosion model.

5.3.4 Total Energy Deposition in the Near Surface Region

The simplest model which can describe a thermal erosion mechanism is one which assumes the yield to be directly proportional to the total energy deposited in the near surface region. The closest agreement obtained with this approach was the erosion behaviour of Xe with ^{4}He irradiation. Helium irradiation of ice deviated from a direct scaling with the total stopping power, and as pointed out earlier, heavy ion results for sputtering of both xenon and ice films did not exhibit a direct energy scaling.

In cases where the nuclear stopping power is dominating, a simple direct scaling is expected to be a much more satisfactory approximation. However, for MeV ion bombardment of frozen gas films almost all deposited energy is in the form of electronic excitation. Experimental results show that the simple linear scaling is in general not sufficient; the nature of the electron-

phonon coupling must play an important role.

5.4 Anomalies in Erosion Behaviour

Several experimental results indicate that the model outlined earlier provides only a general description of the erosion behaviour. Numerical integration with reasonable values of the parameters gave results in the correct order of magnitude. Indeed exact quantitative agreement should not be expected. The model gives an indication of validity and a feeling for dependence of the yield on various parameters.

The negative thickness coefficient observed with ^{4}He irradiation of ice films may be a result of non uniformity at small thicknesses. The angular dependence data indicates that such non uniformities would lead to an enhanced erosion yield. One possible source of non uniformity is the surface of the substrate - in this case Be + 5 nm of copper. However, it had been previously established that films deposited on a Si substrate (optically flat) gave the same results.

The decrease in the sputtering yield of ice at large film thicknesses is also surprising since a saturation level is expected. One possibility is that for

sufficiently large film thicknesses another structure is stabilized, although a conceptual picture of bonding would indicate that this should occur at thicknesses corresponding to no more than a few monolayers. Another possibility is the existence of significant non uniformities up to fairly large coverages. Erents and McCracken[14] observed similar behaviour in a low energy regime although the explanation does not agree with the present interpretation of the mechanism.

The sputtering of ice also exhibits an anomalous negative temperature coefficient indicating a possible structural temperature dependence. Nevertheless, this would involve a transformation after the initial film deposition at 20 K. Two experiments were conducted in which films were deposited at 62 K and 121 K and sputtered at 20 K. A small decrease was observed in the yield from deposition at 20 K (S = 8.9) to 121 K (S = 7.9). The results are not conclusive but they indicate that a structural contribution is not unreasonable.

The energy dependence of the sputtering of ice by ^{4}He irradiation was a monatonically decreasing function of energy whereas the total stopping peaks at 600 keV. As

pointed out previously, the erosion of ice shows that the physical processes do not lend themselves to description by a simple model based on direct scaling with the total energy deposition. Energy deposition on the microscopic scale involves various modes of excitation depending on the ion-target combination and the energy of the incident ion. Hence it is reasonable to suppose that the yield depends on the specific nature of the energy loss and hence the electron-phonon coupling.

It should be realized that the physics of the ice structure is much more complicated than either Xe or Kr. Therefore the xenon experiments should represent a more definitive means of determining the nature of the mechanism. Indeed the helium irradiation of xenon exhibits no anomalies in the temperature, thickness or energy dependence of the yield. The heavy ion results, however, exhibit a nonlinear energy dependence. The ^{14}N yields scaled well with the nuclear stopping power, whereas the ^{40}Ar bombardment, where the nuclear stopping represented a much larger fraction of the total, showed virtually no dependence on the energy of the incident ion. Again the exact nature of the excitation and coupling mechanism must be important.

5.5 Summary of Conclusions

The general features of the temperature and thickness dependence of the sputtering indicate that a thermal mechanism is important for all systems studied. Anomalies in the energy dependence may be explained in terms of a more complex treatment of the microscopic features of energy deposition. Solely such a thermal spike mechanism can even qualitatively explain the erosion yields, exceeding collisional sputtering by orders of magnitude.

Beyond demonstrating the general features of the mechanism, and indicating the magnitude of the yields, further studies should be designed to yield a deeper understanding of the microscopic details of the interaction.

TABLE I

SPUTTERING OF ICE

1(a) THICKNESS DEPENDENCE - ^{4}He IRRADIATION

T = 20 K, ^{4}He Energy = 1 MeV

THICKNESS (units of 10^{15} molecules/cm^2)	SPUTTERING YIELD (atoms/ion)
108	9.8
241	9.1
289	8.9
292	8.8
498	8.2
730	11.7
1417	10.3

TABLE I

SPUTTERING OF ICE

1(b) TEMPERATURE DEPENDENCE - ^{4}He IRRADIATION

^{4}He Energy - 1 MeV

TEMPERATURE (°K)	THICKNESS (units of 10^{15} molecules/cm^2)	SPUTTERING YIELD (atoms/ion)
20*	292	8.8
40	276	7.1
63	307	7.6
82	277	7.8
100	262	10.4
120	261	14.2

* 3 measurements on different days support this value

TABLE I

SPUTTERING OF ICE

1(c) ENERGY DEPENDENCE - ^{4}He IRRADIATION

T = 20 K

ENERGY (keV)	THICKNESS (units of 10^{15} molecules/cm^2)	SPUTTERING YIELD (atoms/ion)
1000	289	8.9
600	296	16.8
300	286	20.1

TABLE I

SPUTTERING OF ICE

1(d) ANGULAR DEPENDENCE - ^{4}He IRRADIATION

T = 20 K, ^{4}He Energy - 1 MeV

TILT ANGLE (degrees, w.r.t. surface normal)	THICKNESS (units of 10^{15} molecules/cm^2)	SPUTTERING YIELD (atoms/ion)
5	292	8.8
25	342	12.0
40	275	15.1
50	344	23.9

TABLE I

SPUTTERING OF ICE

1(e) DEPENDENCE ON DEPOSITION TEMPERATURE

^{4}He IRRADIATION

T(sputtering) = 20 K, ^{4}He Energy = 1 MeV

DEPOSITION TEMPERATURE (°K)	THICKNESS (units of 10^{15} molecules/cm^2)	SPUTTERING YIELD (atoms/ion)
20	289	8.9
62	289	8.4
121	264	7.9

TABLE I

SPUTTERING OF ICE

1(f) HEAVY ION RESULTS

T = 36 K

ION	THICKNESS (INITIAL → FINAL) (units of 10^{15} molecules/cm^2)	SPUTTERING YIELD (atoms/ion)
0.3 MeV ^{40}Ar	291 - 253	190
1 MeV ^{40}Ar	302 - 211	910
1 MeV ^{14}N	279 - 225	540

TABLE II

SPUTTERING OF XENON

2(a) TEMPERATURE DEPENDENCE - ^{4}He IRRADIATION

^{4}He Energy = 1 MeV

TEMPERATURE (°K)	THICKNESS (units of 10^{15} atoms/cm^2)	SPUTTERING YIELD (atoms/ion)
∿15	280	2.6
25	344	5.6
35	291	6.6
36.5	285	10.9
40	296	16.3
45	309	32.8

TABLE II

SPUTTERING OF XENON

2(b) ANGULAR DEPENDENCE - ^{4}He IRRADIATION

T ∿ 15 K, ^{4}He Energy = 1 MeV

ANGLE (degrees, w.r.t. surface normal)	THICKNESS (units of 10^{15} atoms/cm^2)	SPUTTERING YIELD (atoms/ion)
5	291	2.6
20	316	3.4
20*	385	4.0
35	314	4.7
50	319	5.7

* Higher yield probably represents a thickness effect

TABLE II

SPUTTERING OF XENON

2(c) NITROGEN IRRADIATION

ION	THICKNESS (units of 10^{15} atoms/cm^2)	SPUTTERING YIELD (atoms/ion)
600 keV ^{14}N	177	46
1 MeV ^{14}N	167	35
2 MeV ^{14}N	150	19
1.2 MeV $^{14}N_2$	179	41

TABLE II

SPUTTERING OF XENON

2(d) ARGON IRRADIATION

ION	THICKNESS (units of 10^{15} atoms/cm^2)	SPUTTERING YIELD (atoms/ion)
600 keV ^{40}Ar	318	321
1 MeV ^{40}Ar*	299	290
1 MeV ^{40}Ar	324	258
1.5 MeV ^{40}Ar	300	249
2 MeV ^{40}Ar	288	277

* One half of the film was eroded in the measurement

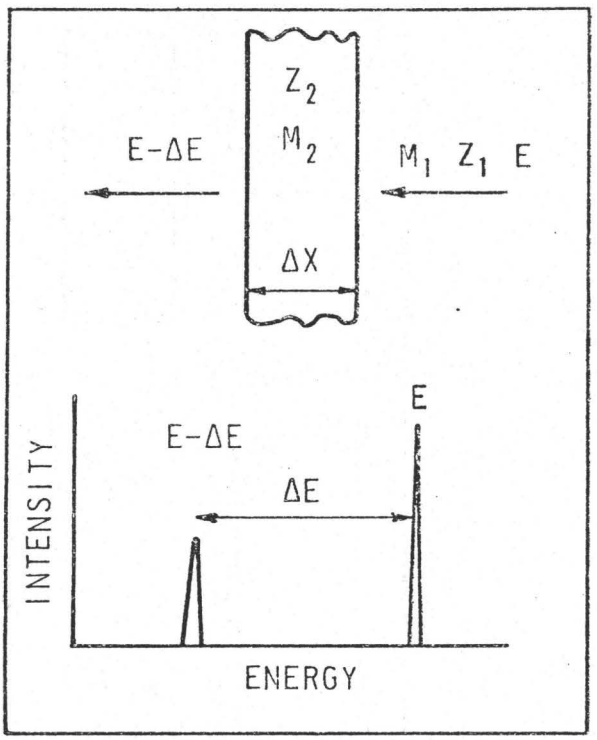

Figure 1(a) Energy Loss with Ion Penetration

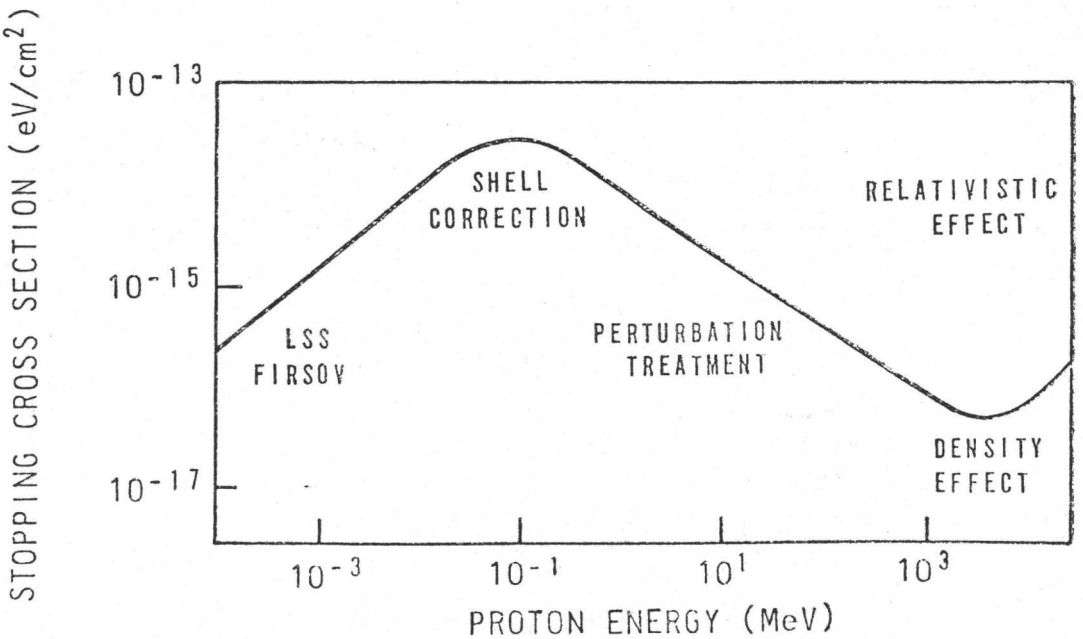

Figure 1(b) General Features of Energy Loss

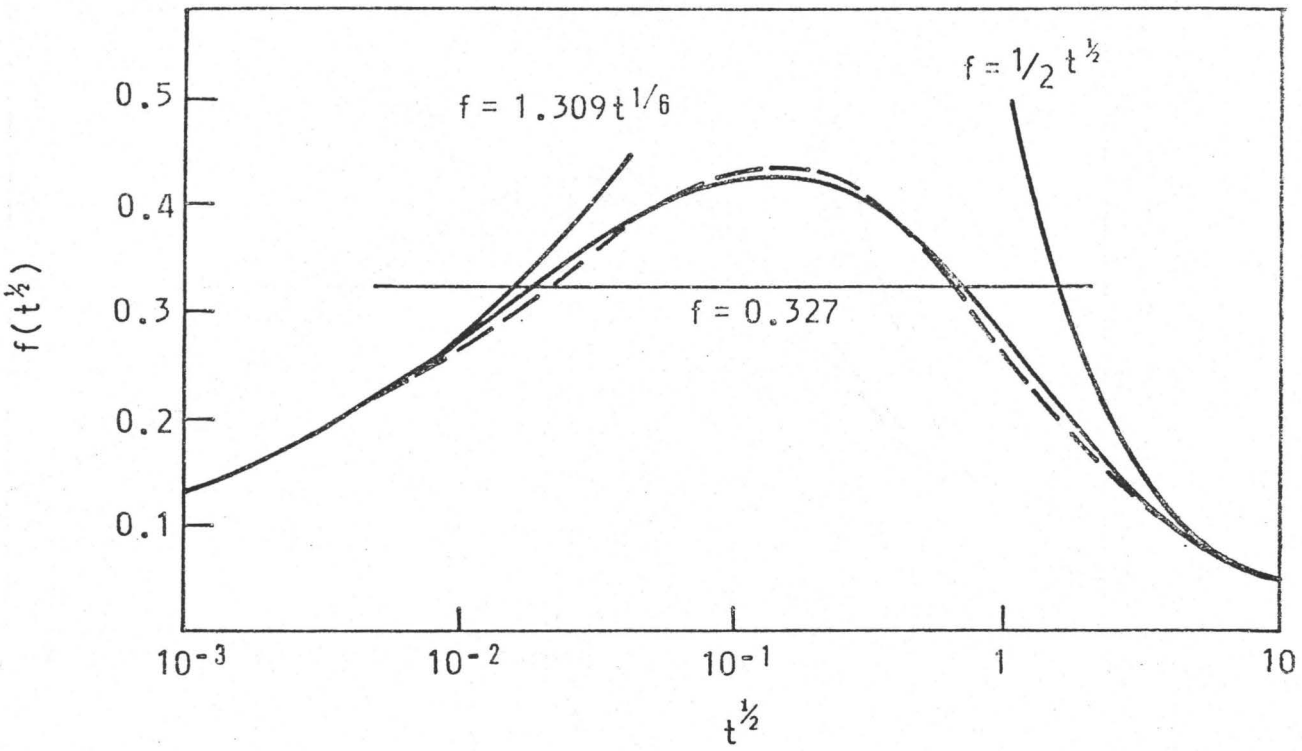

Figure 2(a) The Universal Screening Function

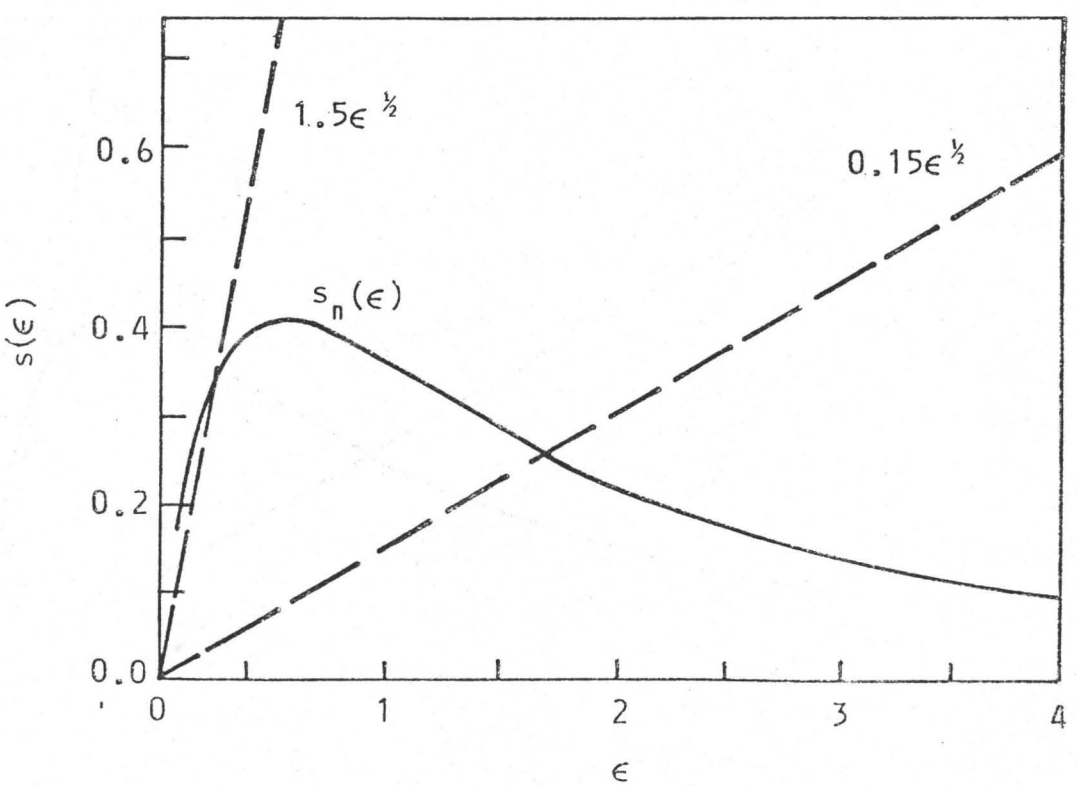

Figure 2(b) The Universal Nuclear Stopping Cross Section

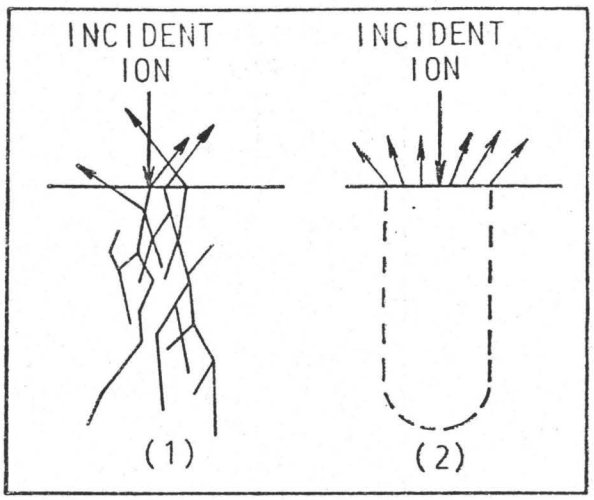

3(a)(1) Collisional Atomic Ejection
3(a)(2) Evaporation from a "Thermal Spike"

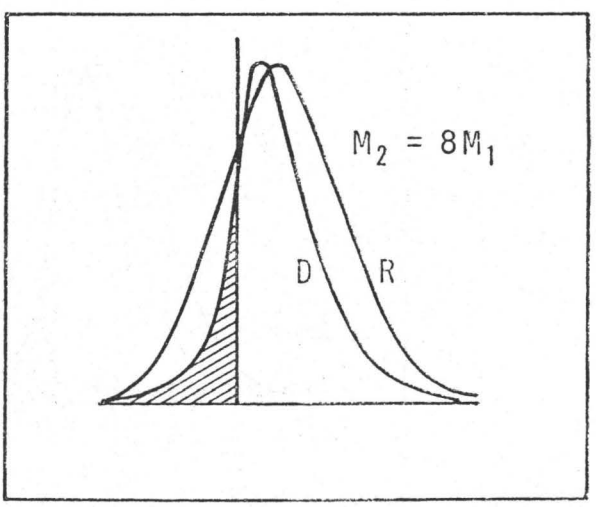

Figure 3(b) Statistical Damage and Range Distributions

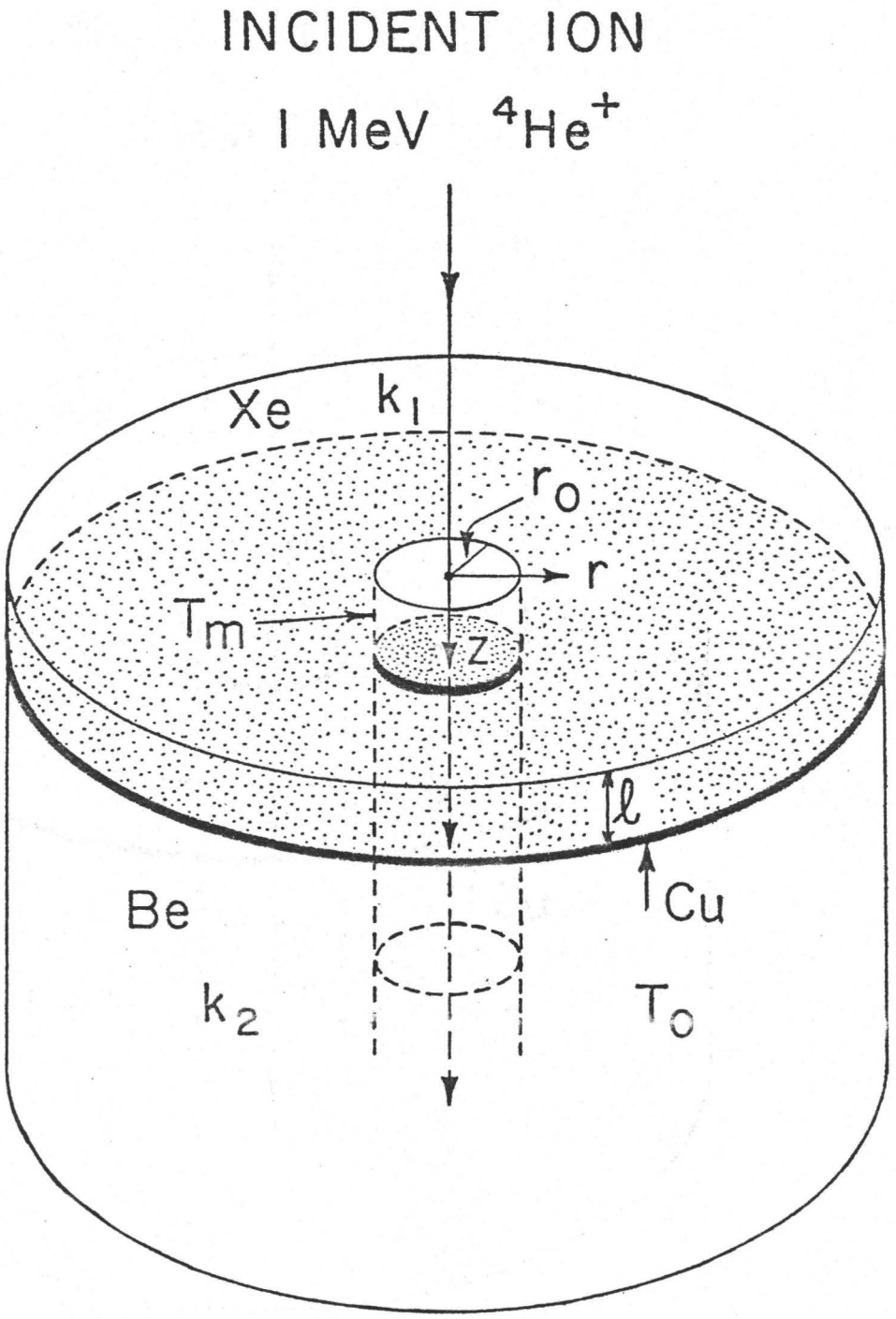

Figure 4 A Cylindrical Energy Spike

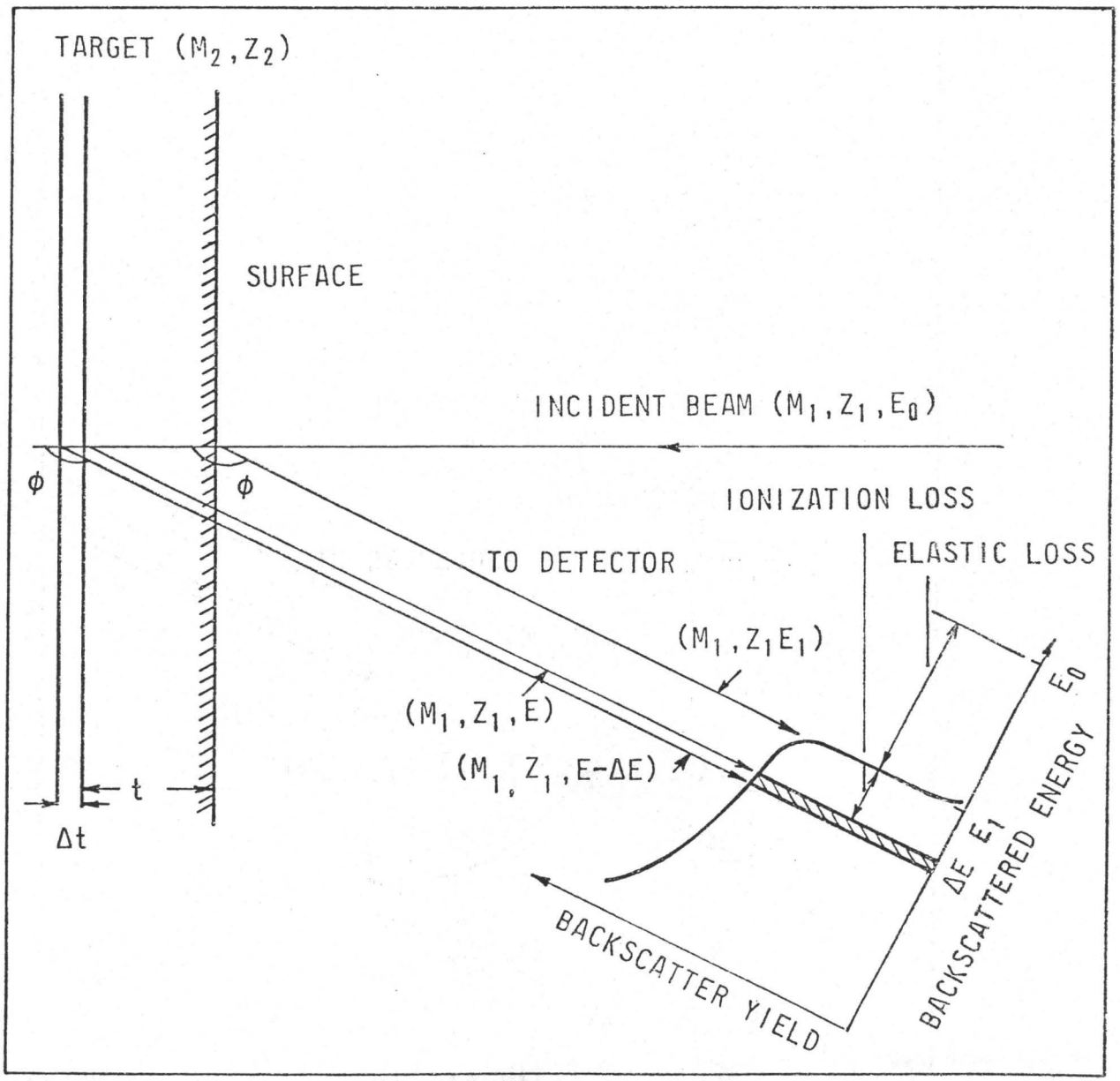

Figure 5 Rutherford Backscattering Spectrometry

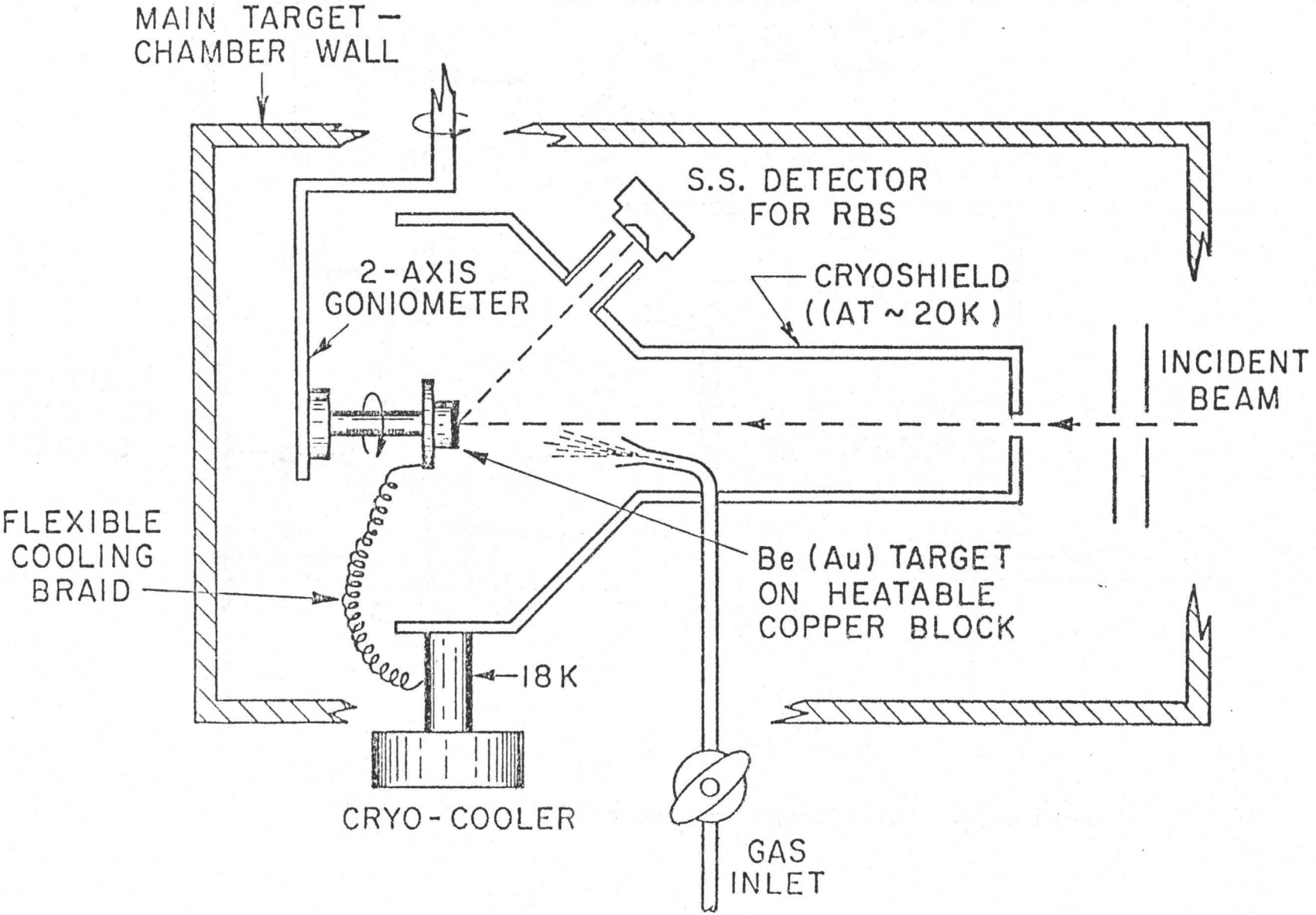

Figure 6 Target Chamber for the 2.5 MeV Van de Graaff

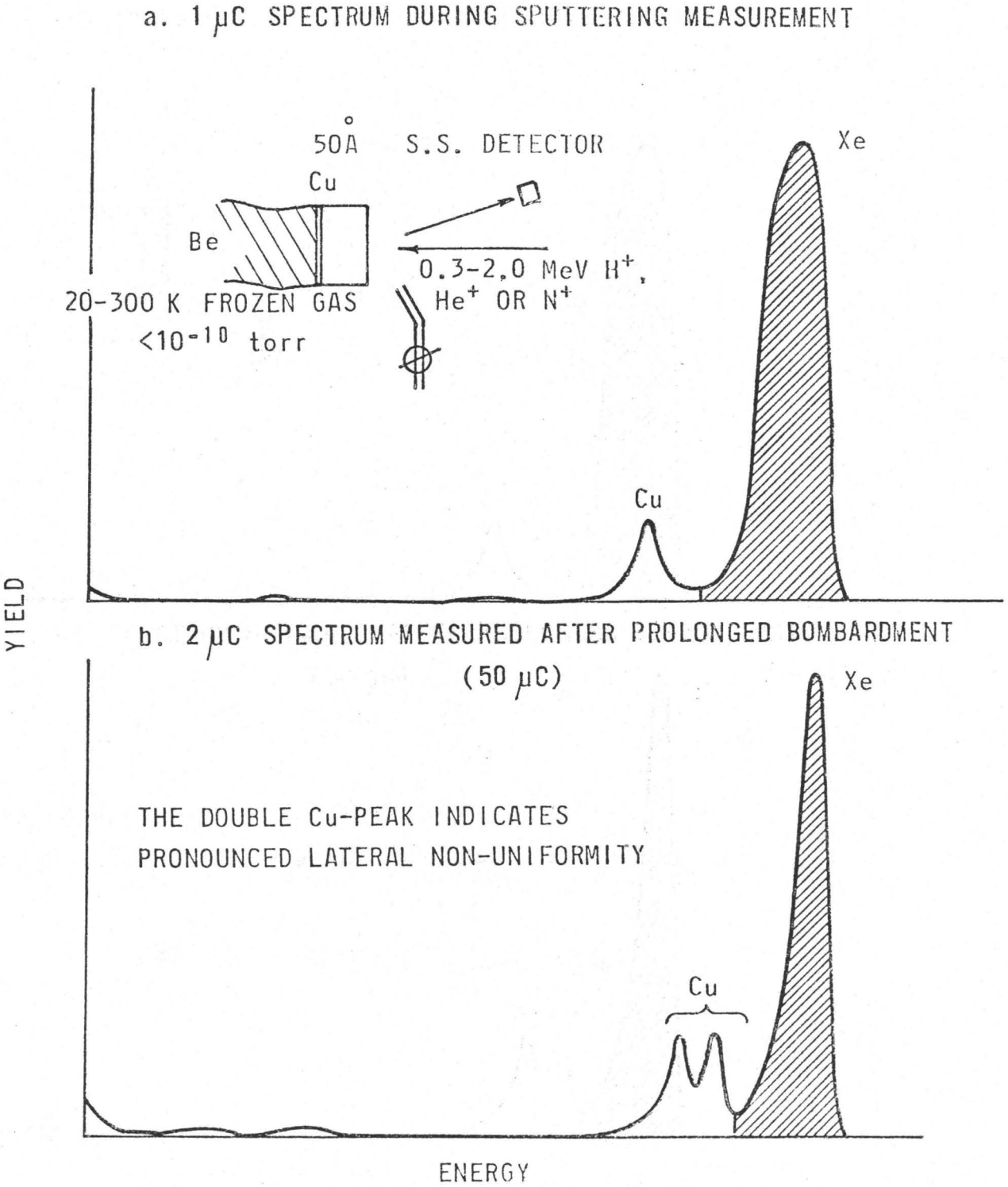

Figure 7(a) Typical Xe Spectrum
Figure 7(b) Spectrum After Prolonged Bombardment

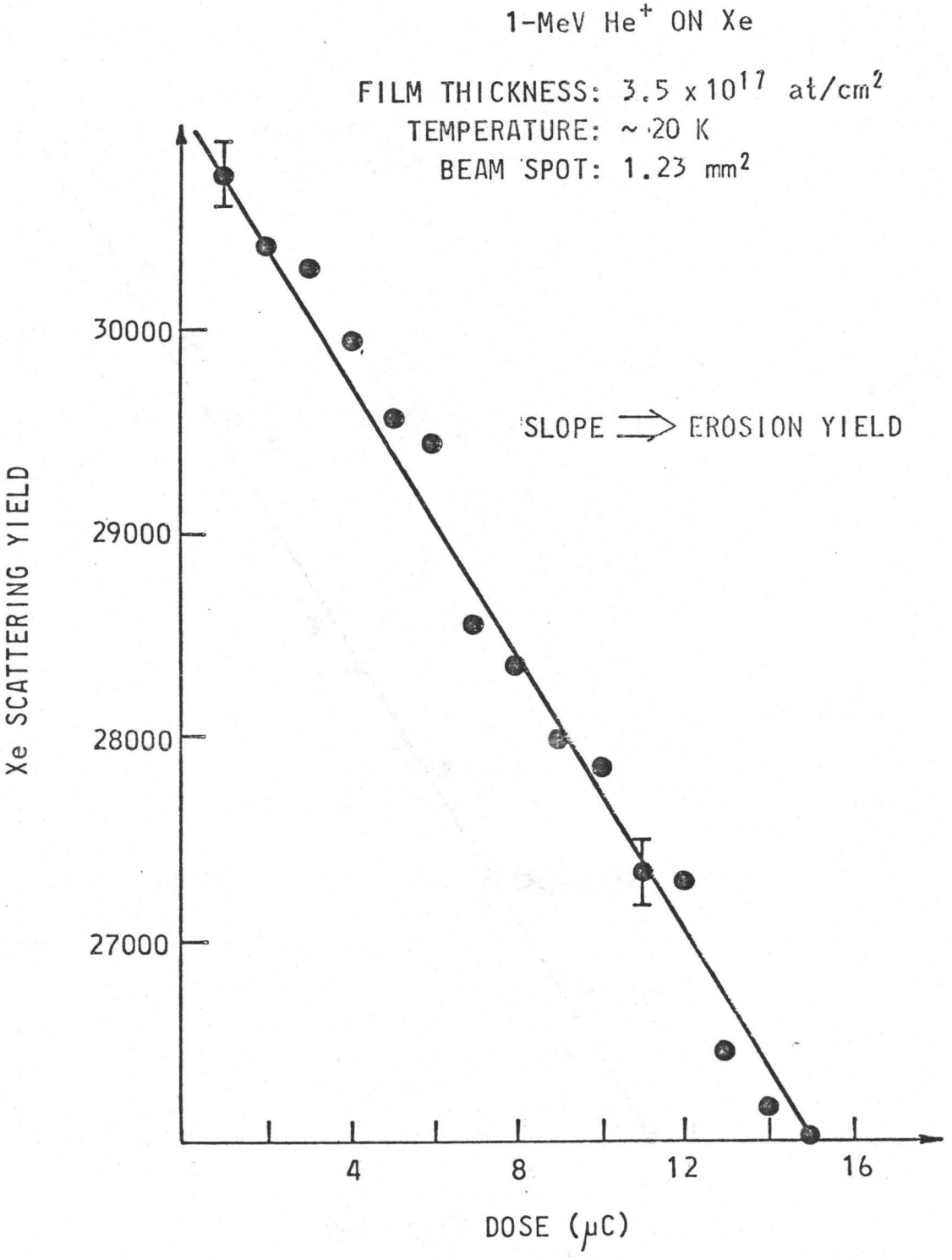

Figure 8 Data Reduction from Backscattering Yield

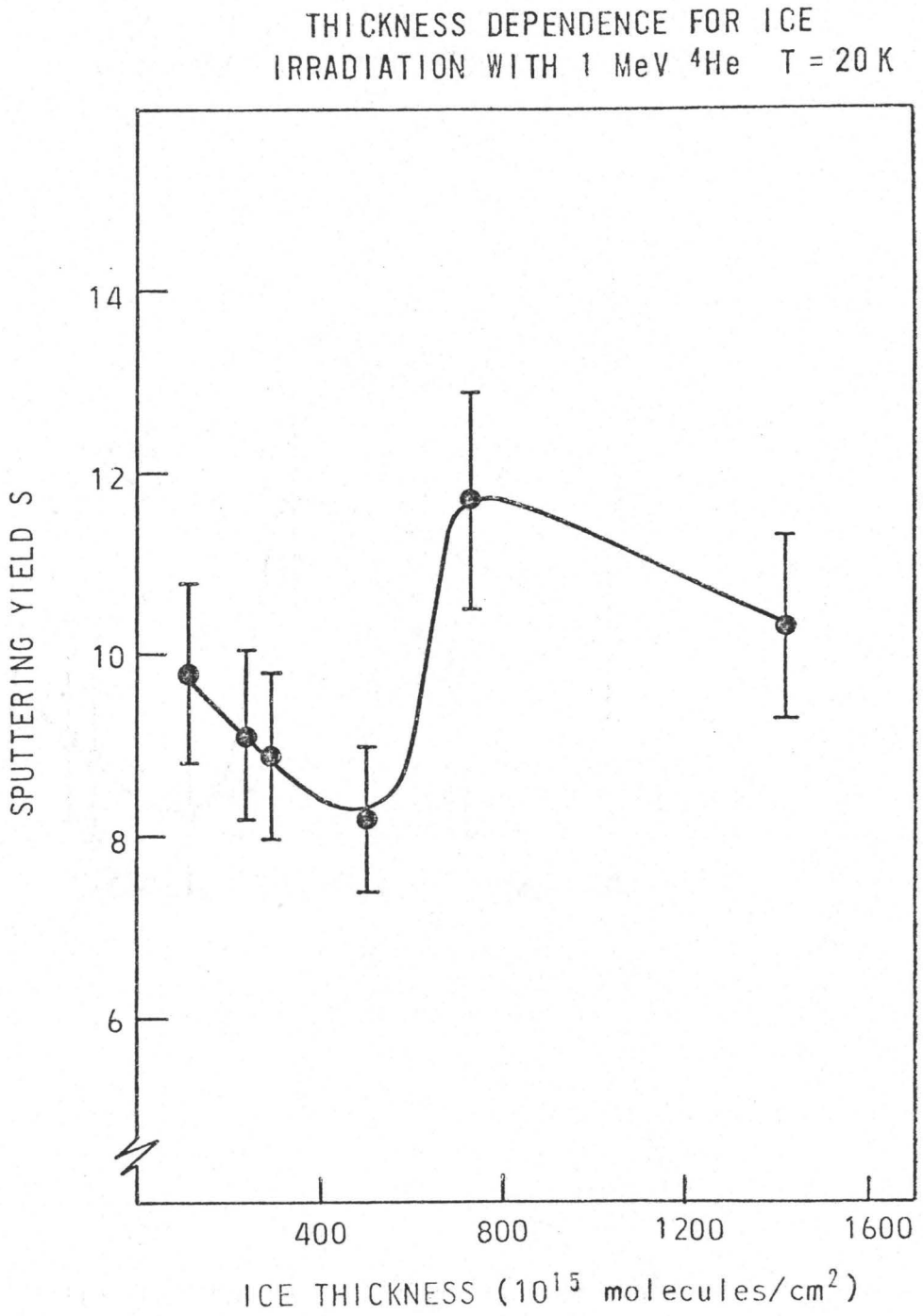

Figure 9 Thickness Dependence for Sputtering of Ice

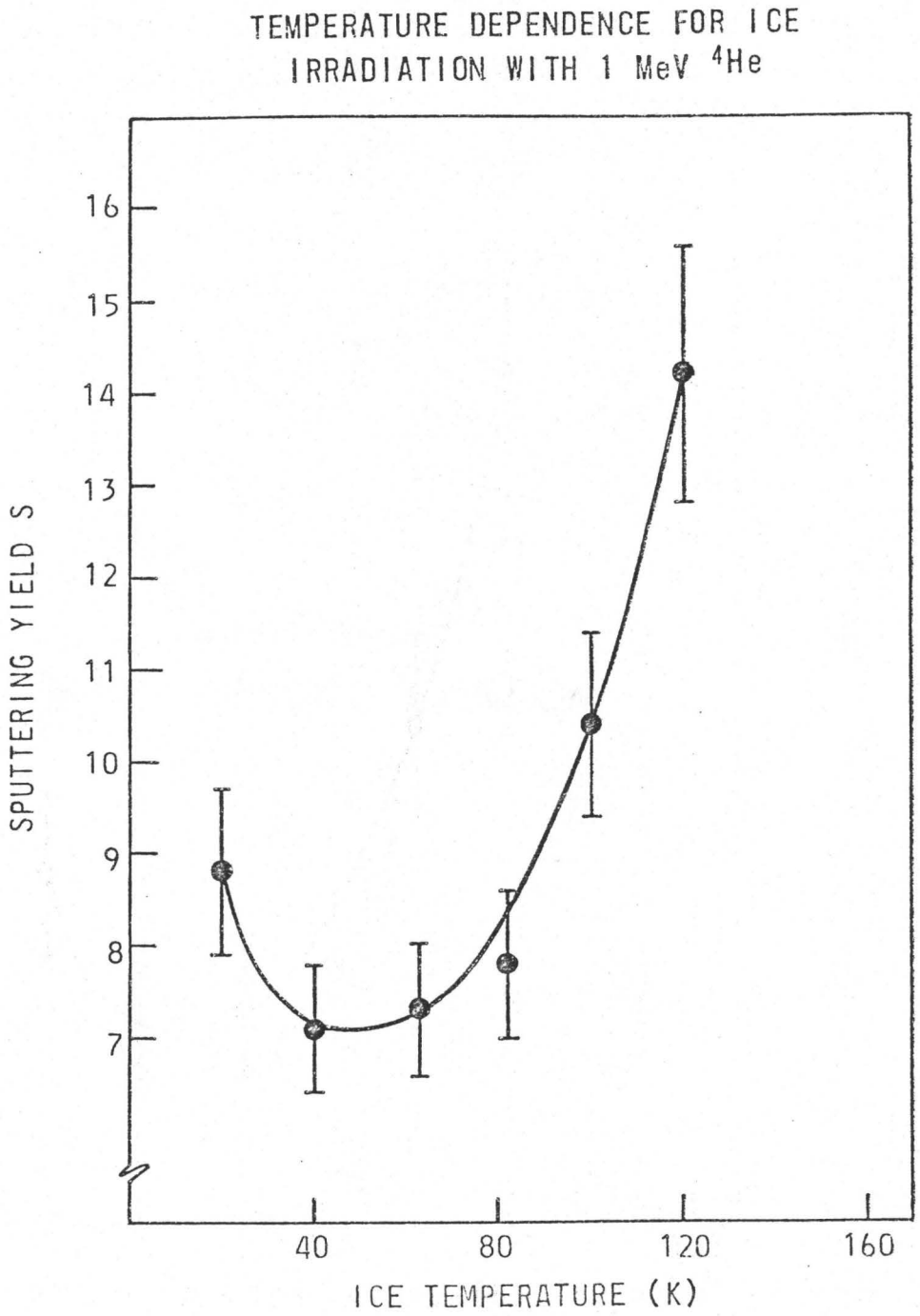

Figure 10 Temperature Dependence for Sputtering of Ice

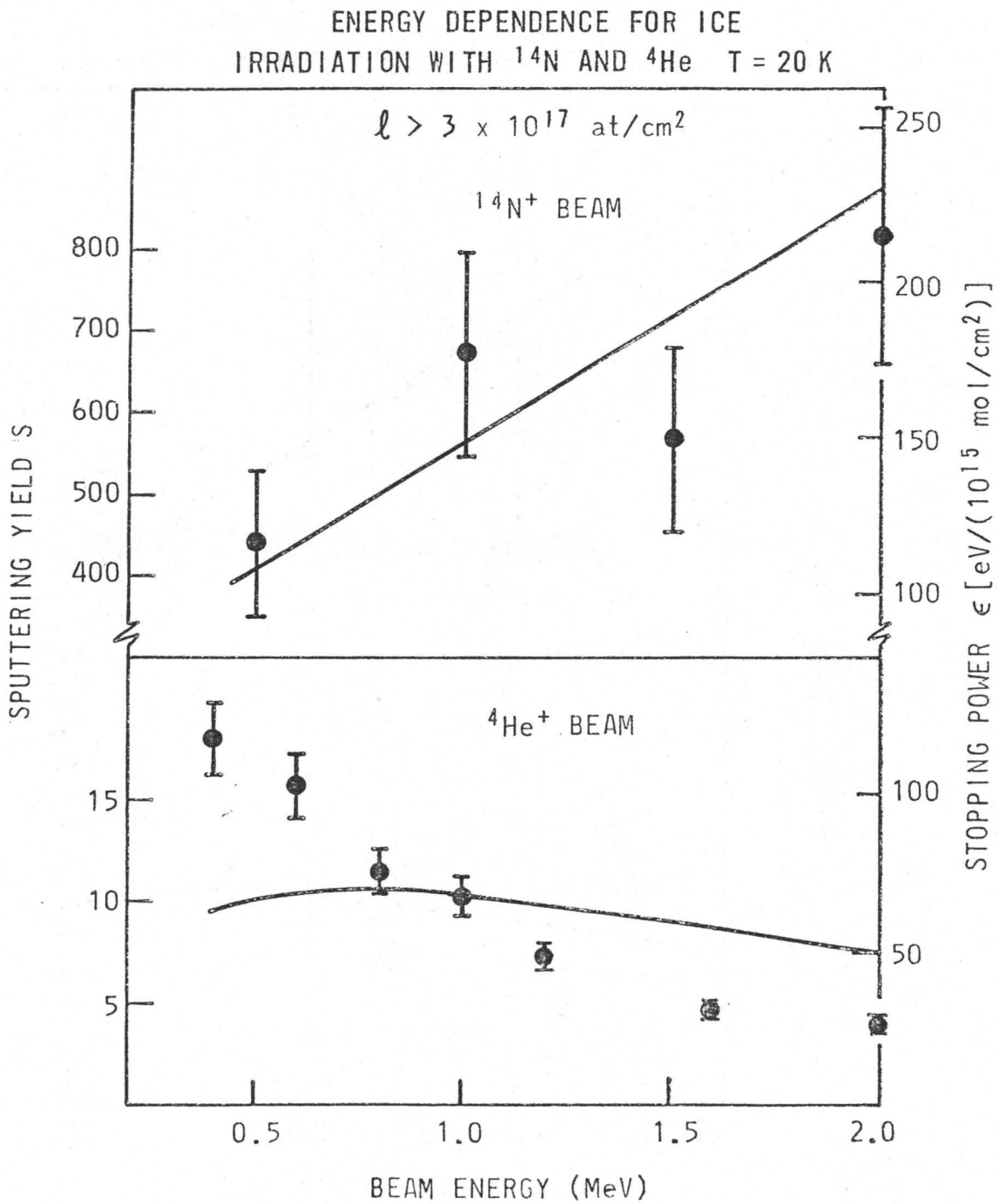

Figure 11 Energy Dependence for Sputtering of Ice

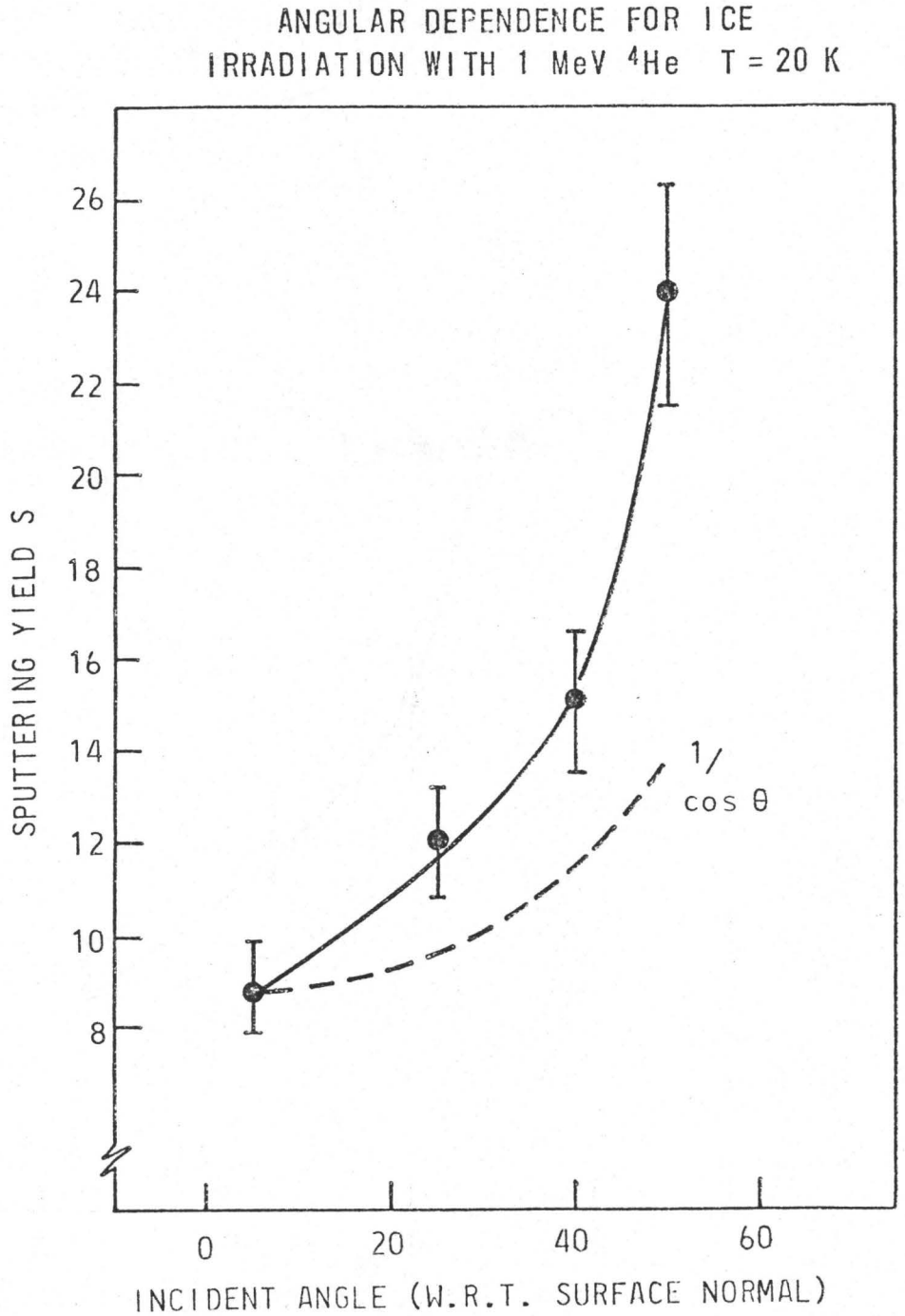

Figure 12 Angular Dependence for Sputtering of Ice

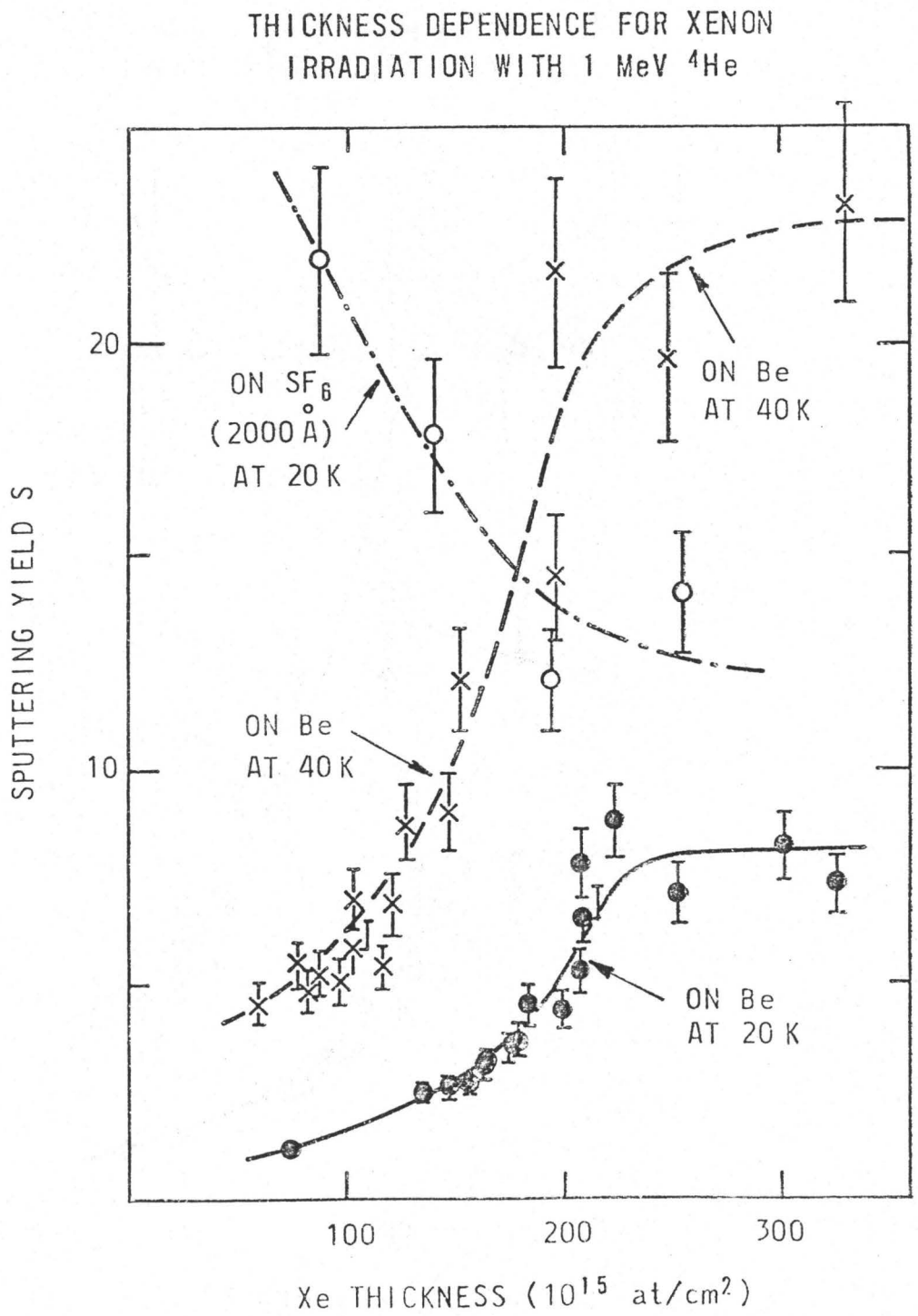

Figure 13 Thickness Dependence for Xe Sputtering

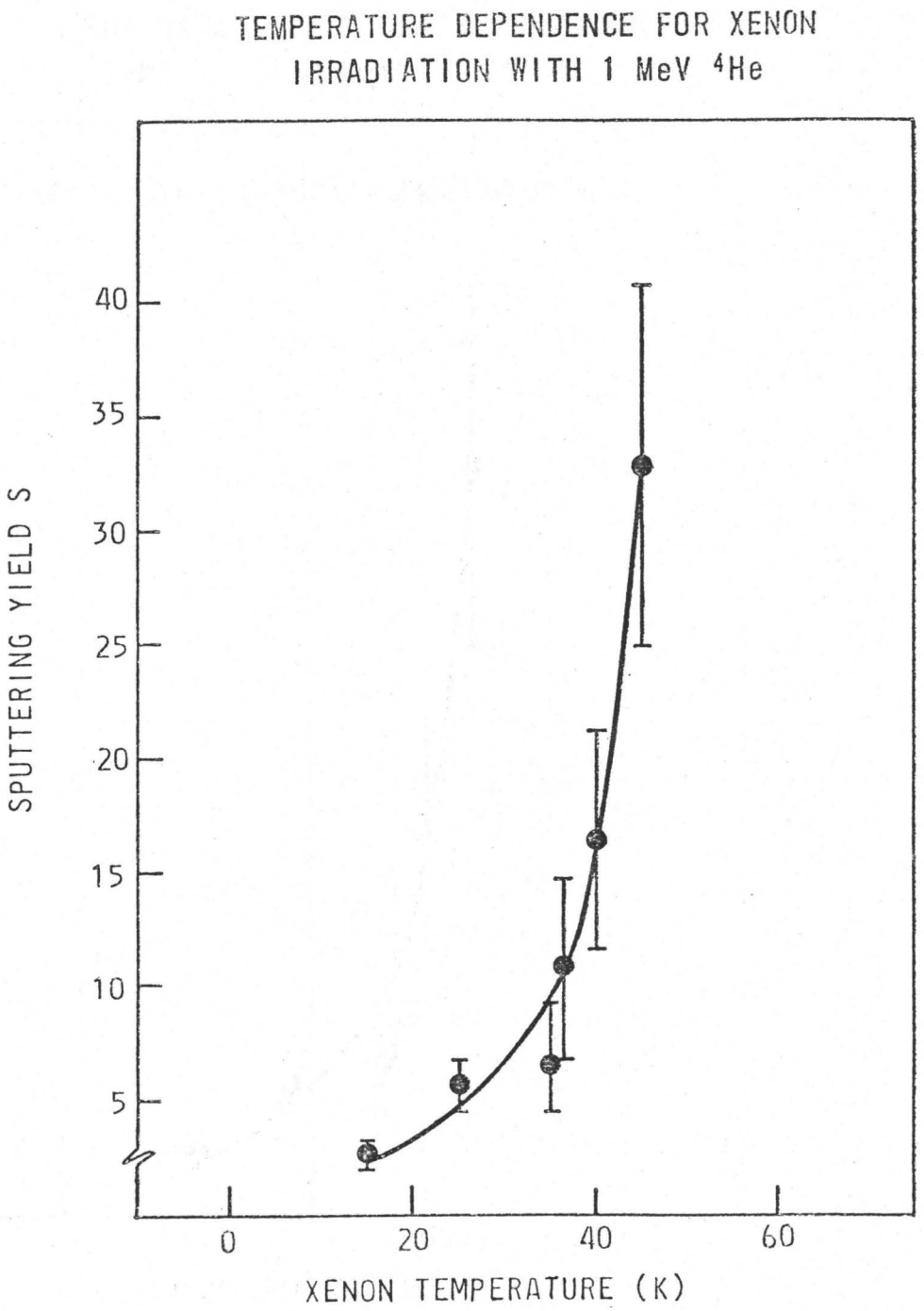

Figure 14 Temperature Dependence for Xe Sputtering

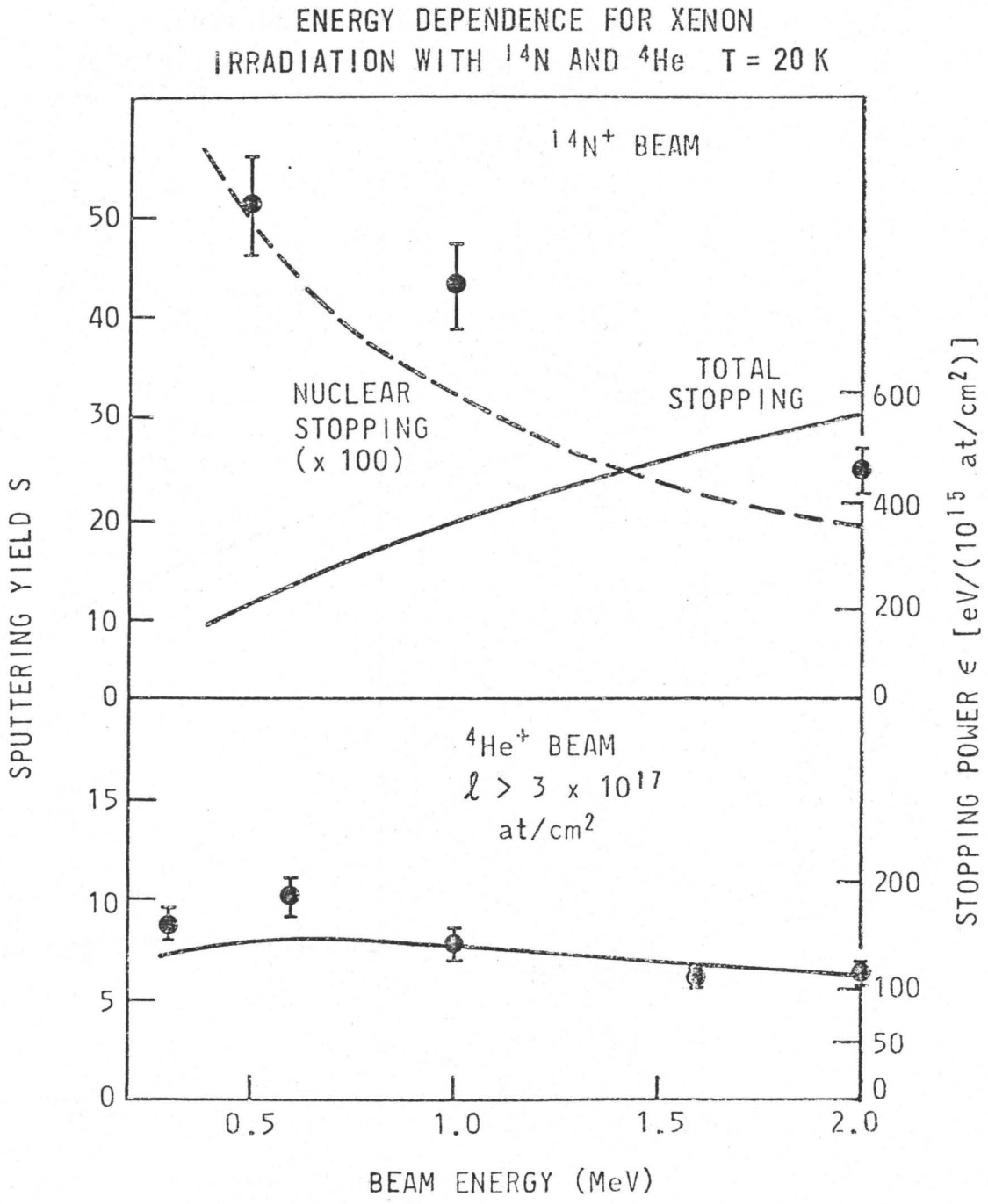

Figure 15 Energy Dependence for Xe Sputtering

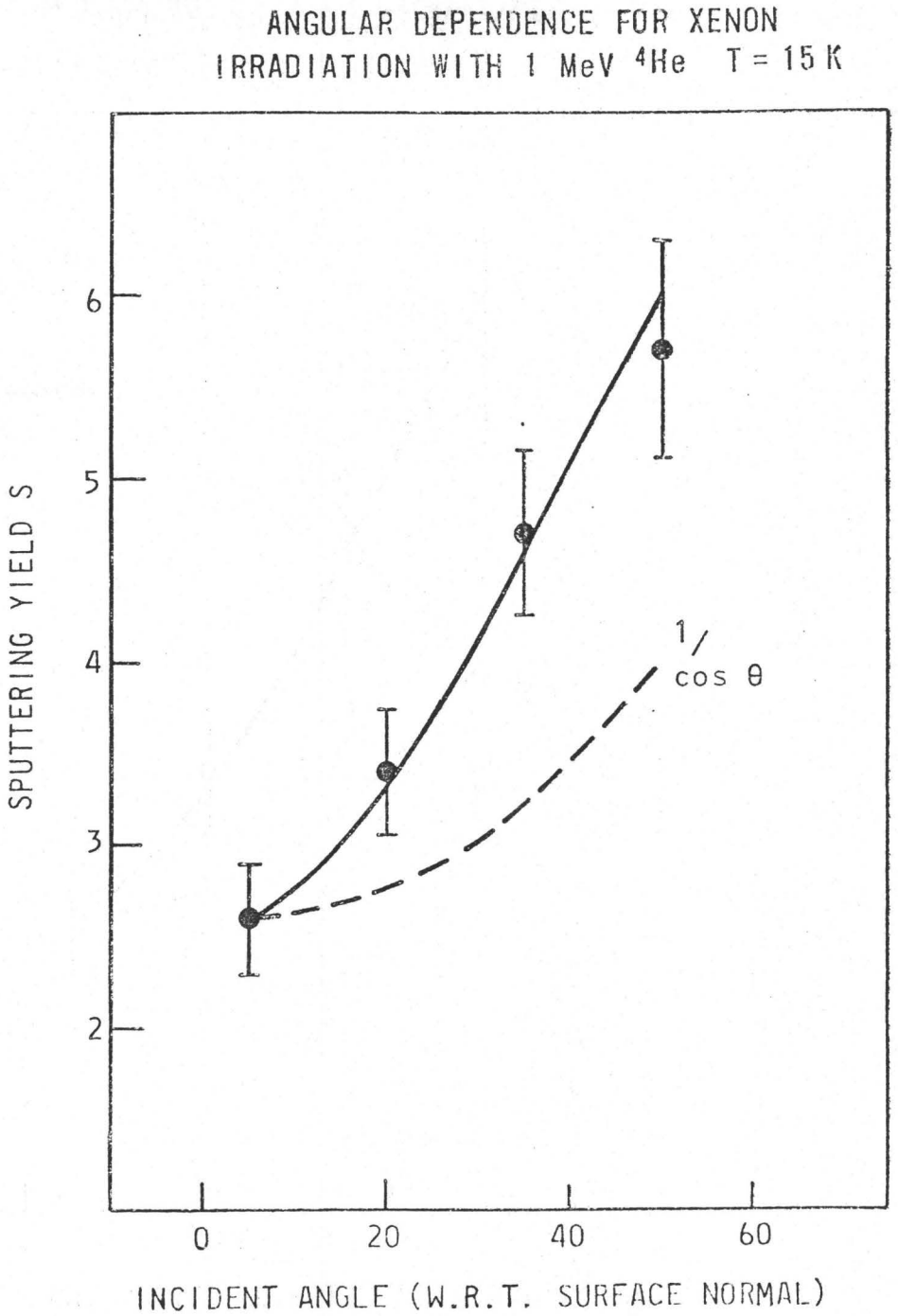

Figure 16 Angular Dependence for Xe Sputtering

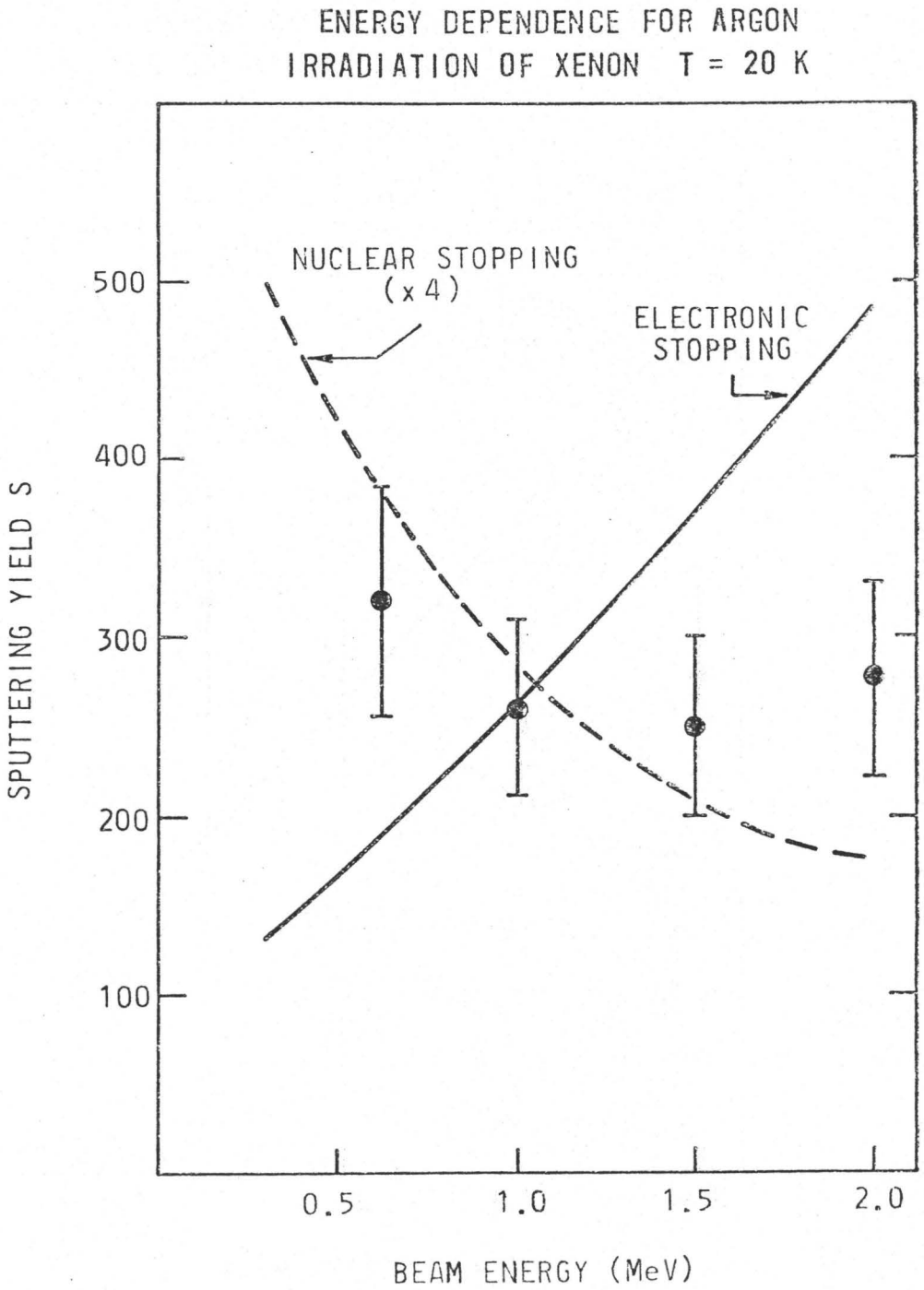

Figure 17 Sputtering of Xe by ^{40}Ar

REFERENCES

1. P. Sigmund, Phys. Rev. 184, No. 2, 383 (1969).

2. J.A. Davies, *et al.*, Proceedings of Int. Conference on Ion Implantation in Semiconductors, Budapest, Hungary (1978).

3. J. Lindhard, *et al.*, Kgl. Dan. Vid. Selsk. Mat. Fys. Medd. 33, No. 10 (1963).

4. O.B. Firsov, Engl. Transl. Sov. Phys. JETP 9, 1076 (1959).

5. H.A. Bethe, Intermediate Quantum Mechanics. Benjamin, New Yrok, Amsterdam, Ch. 15.

6. U. Fano, Ann. Rev. Nucl. Sci. 13, 1 (1963).

7. M. Inokuti, Rev. Mod. Phys. 43, 297 (1971).

8. J.F. Ziegler, Stopping Powers and Ranges in All Elements, Vol. 4, First Edition, Pergamon (1977).

9. L.C. Northcliffe and R.F. Schilling, Range and Stopping Power Tables for Heavy Ions, Nuclear Data Tables A7, Academic Press (1970).

10. J. Lindhard, *et al.*, Kgl. Dan. Vid. Selsk. Mat. Fys. Medd. 36, No. 10 (1968).

11. R. Kelly, Radiation Effects 32, 91 (1977).

12. J. L'Ecuyer, submitted to Nuclear Instruments and Methods.

13. D.A. Thompson and S.S. Johar, submitted to Applied Physics Letters.

14. S.K. Erents and G.M. McCracken, J. Applied Physics 44, No. 7 (1973).